Experimental results on the stabilization of lifted jet diffusion flames

By L. K. Su, D. Han AND M. G. Mungal

1. Motivation and objectives

Many researchers have studied the stabilization of lifted turbulent jet diffusion flames. Earlier work in this area was thoroughly reviewed by Pitts (1988). Recent advances in laser diagnostic methods have vastly increased the breadth of data available regarding this problem, while increased computational capacity has permitted the assessment of various models for flame stabilization. However, there remains no consensus regarding the stabilization mechanism.

Proposed models differ primarily on the role of premixing at the flame front. Given a jet of undiluted fuel issuing into air, it is undisputed that some degree of fuel-air premixing occurs upstream of the lifted flame. The stabilization theory of Vanquickenbourne & van Tiggelen (1966) assumed full premixedness of fuel and air at the stabilization point, with stabilization occurring through a balance of the local jet axial velocity and turbulent flame speed. Subsequently, Peters & Williams (1983) argued that, in axisymmetric turbulent jets, insufficient molecular mixing occurs upstream of the flame front to support the notion of premixed flame propagation. Instead, stabilization was proposed to be governed by the quenching of thin, laminar diffusion flamelets. Müller *et al.* (1994) later extended this work to consider partially premixed flamelets, concluding again that flamelet quenching was important to flame stabilization.

Recently, triple flame theories (Dold (1989), Veynante *et al.* (1994), Ruetsch *et al.* (1995)) have been applied to the stabilization problem. Essential to the formation of the triple flame structure is a gradient in the fuel mixture fraction profile normal to the flow direction, ranging from fuel-rich to fuel-lean conditions across the profile. On either side of the stoichiometric point, a premixed flame branch forms. The excess fuel and oxidizer from the rich and lean branches, respectively, then burn as a downstream diffusion flame. These three structures – the rich and lean premixed branches and the diffusion tail – motivate the 'triple flame' nomenclature. In the idealized case of a uniform incoming velocity profile, the premixed branches present a convex surface to the flow, with the fuel-rich and fuel-lean sides receding owing to the reduced flame speed with departure from stoichiometry. The addition of the diffusion tail downstream of this convex surface results in the characteristic triple flame shape, which resembles a boat anchor. In a lifted turbulent jet flame, however, the incoming velocity profile can be expected to be highly non-uniform. Veynante *et al.* (1994) computed triple flames with vortices superposed on the incoming velocity profiles. Under these conditions the flame branches are highly distorted from the idealized shape. For sufficiently high strain rates, one of the premixed branches may be extinguished while the other branches continue to burn. Because of these departures from the idealized triple flame structure, the term 'leading-edge flame'

or 'edge flame' is preferred when describing flame stabilization involving upstream partial premixing with a trailing diffusion flame branch.

Emergence of the edge flame theory of flame stabilization has been coincident with the extensive application of planar laser diagnostic methods to the problem. Measurements have been presented of mixture fraction, scalar dissipation rate, and temperature fields (Schefer *et al.* (1994), Kelman *et al.* (1998)), reaction zone locations (Maurey *et al.* (1998), Schefer & Goix (1998), Watson *et al.* (1999a), Watson *et al.* (1999b)), and fluid velocities in and around the reaction zones (Muñiz & Mungal (1997), Maurey *et al.* (1998), Schefer & Goix (1998), Watson *et al.* (1999a)). The mixture fraction and dissipation measurements of Schefer *et al.* (1994) show scalar dissipation rates well below quenching values at the flame stabilization points, indicating that scalar dissipation is not significant to the stabilization process for the lifted methane flames studied, in contradiction to the model of Peters & Williams (1983). The velocity measurements of Muñiz & Mungal, conditioned on flame location, show that the flame stabilizes in regions of low incoming fluid velocity (typically less than three times the laminar flame speed, S_L). This, together with velocity profiles normal to the flame base and streamline patterns in the upstream region, suggests triple flame behavior similar to that seen in the computations of Ruetsch *et al.* (1995). Using measurements of CH radical concentrations to locate reaction zones, Watson *et al.* (1999b) show evidence of both the lean premixed branch and diffusion tail of the idealized triple flame. It is hypothesized that the rich premixed branch is folded into the diffusion tail in the manner suggested by the simulations of Veynante *et al.* (1994).

The conclusions drawn from these experimental studies all have some degree of uncertainty, however, stemming from experimental limitations. Complete elucidation of the stabilization process in the context of the proposed models requires simultaneous knowledge of the reaction zone position, the local velocity field, and the local mixture fraction field; in the studies mentioned, at most two of these were measured. In particular, simultaneous measurements of mixture fraction and velocity have not been demonstrated. The current experiments address this by presenting simultaneous measurement of fuel concentration, using planar laser-induced fluorescence (PLIF) of acetone seeded into the fuel stream, and velocity, measured using particle image velocimetry (PIV), in the stabilization region of a lifted methane-air turbulent jet diffusion flame. The reaction zone can also be fairly well located by these measurements, as will be shown.

2. Results

Much of this work was presented earlier in Su, Han & Mungal (2000). More extensive experimental details can be found in that paper. That paper also contains several figures that have been omitted here for brevity.

2.1. *Experimental arrangement and image interpretation*

The experiments are performed in a vertical wind tunnel which provides a coflow velocity of 0.36 m/s. The methane fuel stream issues from a straight pipe (inner diameter 4.6 mm) placed in the center of the tunnel. Two cases are considered here. In the first, the jet exit speed is 15.3 m/s, giving a jet Reynolds number (based on jet excess velocity, nozzle diameter and methane kinematic viscosity) of roughly 4000. In the second case, the jet exit speed is 10.8 m/s, giving a Reynolds number of roughly 2800. A total of 103 and 88 velocity/scalar image pairs are available for the two cases, respectively.

To provide the Mie scattering signal for the PIV, the coflow air is seeded with a

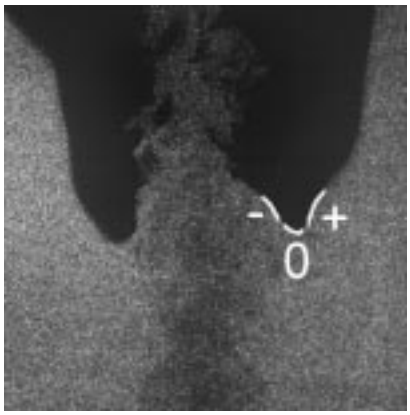

FIGURE 1. A sample Mie scattering field, showing the loss of signal in regions where the glycerol-water particles have evaporated at high temperatures.

glycerol-water fog. A dual cavity Nd:YAG laser, with 532 nm output, is used to produce two pulses with a temporal spacing of 30 μs. The resulting scattering signal is collected by an interline transfer CCD camera (1008 x 1016 pixel resolution) which allows each of the two laser sheet pulses to be captured in a separate image. The cross-correlation PIV algorithm used (Hasselbrink (1999)), which incorporates iterative interrogation window offset (Westerweel *et al.* (1997)), offers high resolution and vector yield. The final processing step yields a 100×100 grid of velocity vectors.

For the PLIF, acetone is seeded into the methane fuel stream, to approximately 15% by volume. A XeCl excimer laser with 308 nm output excites the fluorescence. The resulting signal is captured by a low-noise, high-sensitivity CCD camera, with 515×650 pixel resolution. An optical filter isolates the fluorescence signal from ambient light and flame luminosity. The field of view of the PLIF measurements spans from the jet nozzle exit to a maximum of 18.2 jet diameters, d, downstream, and extends up to 7.3 d to either side of the centerline. It is necessary to include the potential core in the PLIF images in order to correlate signal levels with absolute fuel concentration. No such constraint exists with the PIV, so the PIV imaging windows were placed so as to capture only the flame base region. For case 1, the PIV window spanned from 9.5 to 17.3 d downstream of the nozzle, while for case 2 the PIV window spanned from 6.2 to 15.0 d.

The use of glycerol-water fog particles in lifted flame experiments has previously been demonstrated (Hasselbrink & Mungal (1998)). A sample Mie scattering image, from case 2, is given in Fig. 1. The fog particles evaporate in the range 400-450 K, so the regions with no Mie scattering signal can be interpreted as having been heated by the flame. Because the reaction zone is known to be thin (Watson *et al.* (1999a) report CH regions with an average thickness of approximately 1 mm), the reaction zone can be assumed to follow closely the heated region outlined as in Fig. 1. Analogous to edge flame theories, previous researchers have assumed that the stabilization point of the lifted flame corresponds to the base (i.e. the most upstream position) of the region of elevated temperature. However, Watson *et al.* (1999a), through simultaneous measurements of OH and CH radical concentrations, cast some doubt on this assumption. The CH radical is a short-lived reaction intermediate and is believed to mark accurately the instantaneous

reaction zone, while the OH radical is removed by relatively slow three-body reactions and marks regions containing hot combustion products. Watson *et al.* observed that the thin CH zones tend to lie to the inside (toward the centerline) of the broader OH zones, and in fact presented some sample images in which the OH zones extend upstream of the CH zones. This implies that the base of the high temperature regions in Fig. 1 cannot be unambiguously interpreted as the flame base. In the present work we make use of the simultaneous information on fuel concentration provided by the acetone PLIF. As a necessary condition for any point on the temperature interface delineated in the Mie scattering signal to represent an instantaneous flame location, the fuel concentration immediately upstream of that point must be within the flammability limits.

The use of acetone PLIF as a fluid concentration diagnostic in combustion experiments proceeds with some caveats. One consideration is that acetone decomposes in the flame zones, confining information on fuel concentration to the flame upstream region. Another consideration is the variation in acetone fluorescence yield with temperature. Thurber (1999) found that, for constant pressure and constant laser excitation energy at 308 nm, the measured fluorescence per unit acetone mole fraction at 330 K is 0.938 (normalized by the value at 296 K), dropping to 0.875 at 374 K, and 0.806 at 424 K, which is roughly the temperature marked by the abrupt drop in the Mie scattering signal. Finally, differential diffusion effects may arise in attempting to use acetone to mark the methane fuel stream. In combustion, differential diffusion is thought to be significant because the diffusivity coefficients of hydrogen and heavier species can differ by up to an order of magnitude and because local laminarization by heat release increases the importance of molecular diffusion relative to turbulent transport (Bilger (1982)). Because we are concerned only with the non-burning region of the lifted flame and because the acetone- air and methane-air diffusion coefficients vary by only a factor of two (Reid *et al.* (1987)), we assume here that the effect of differential diffusion is negligible.

2.2. *Data analysis*

Figure 2 shows the measured scalar field corresponding to the Mie scattering field of Fig. 1. Overlaid on the scalar field are the temperature interface determined from the Mie scattering field as well as the boundary of that field. The scalar field shown is the fuel mole fraction, X_f, which corresponds directly to the measured fluorescence. In the unburned gases, the mixture fraction and fuel mass fraction are equivalent and relate to X_f as

$$Z = \frac{X_f M_f}{X_f M_f + (1 - X_f) M_{air}} \tag{2.1}$$

where the M are the molecular masses.

Because the jet-to-coflow velocity ratio is relatively high in these measurements (over 40:1 for case 1 and roughly 30:1 for case 2), the scalar field upstream of the flame should obey pure jet scalings. Figure 3 shows the evolution of flow width for the two cases, where $\delta(x)$ is defined as the full width of the mean radial profile between the 10% points. The width, δ, manifests the expected linear dependence on x for each case until a critical value of x is reached where this trend is broken, caused (as will be confirmed below) by the presence of the flame. Recall that in the flame zones, the acetone fluorescence no longer marks the fuel. The mean radial profiles themselves converge quickly to the Gaussian shape characteristic of jets (figure not shown). The downstream decay appears to attain the expected $1/x$ dependence, though this is not conclusive because of the limited downstream extent of the present measurements (Fig. 4). The decay curves in

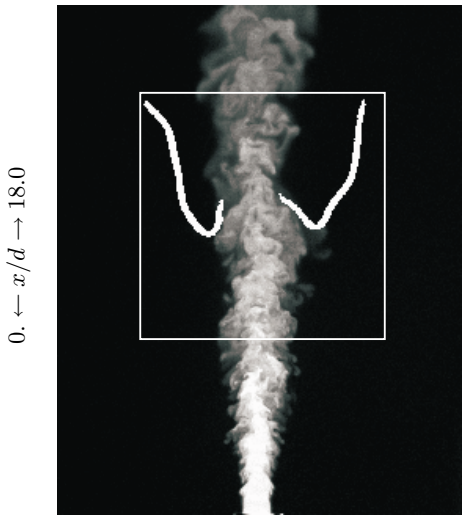

FIGURE 2. The fuel mole fraction field, X_f, (logarithmic grayscale) corresponding to the Mie scattering field of Fig. 1. The PIV imaging window is superimposed on the image, as is the high temperature interface determined from Fig. 1.

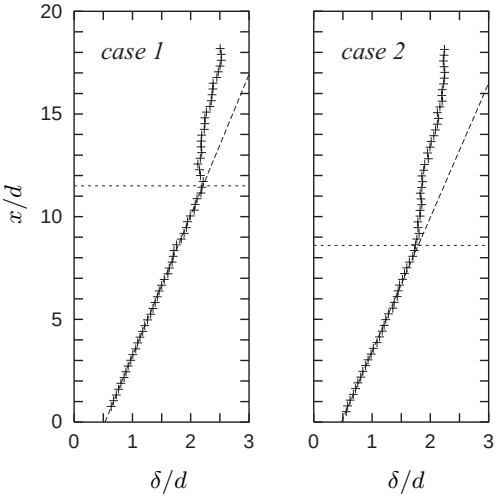

FIGURE 3. Evolution of the scalar flow width for the two cases.

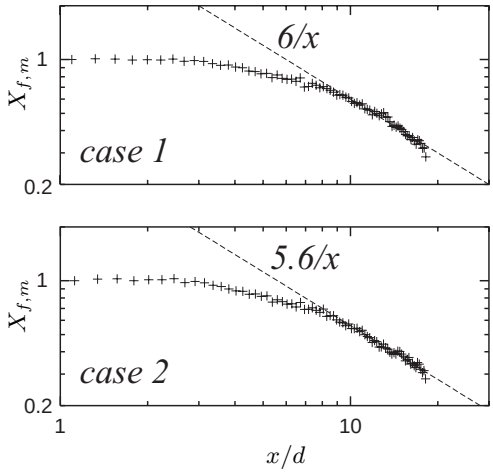

FIGURE 4. Evolution of the centerline scalar decay for the two cases.

Fig. 4 show no evidence of large drops in signal level which would be consistent with the presence of flame surfaces, indicating that the average flame position has not yet migrated to the centerline for the downstream positions shown.

As a first step in determining flame base locations, the temperature gradient interface is found from the Mie scattering images of the form shown in Fig. 1, and this interface is then mapped onto the scalar field image as demonstrated in Fig. 2. The most upstream points of these interfaces (in the following discussion, we will refer to these as the leading

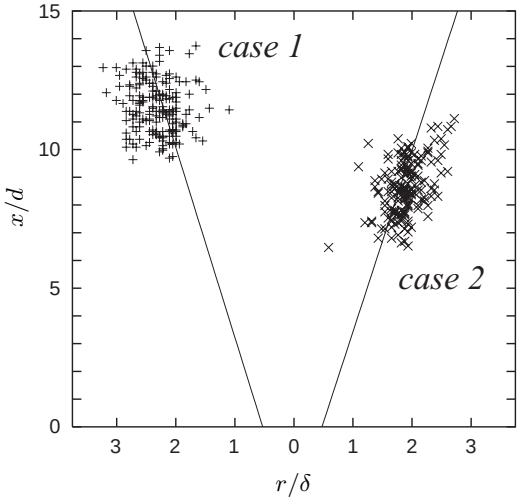

FIGURE 5. Scatterplot of the most upstream points of the high temperature interfaces (the leading points). Lines are the fits to the δ curves of Fig. 3.

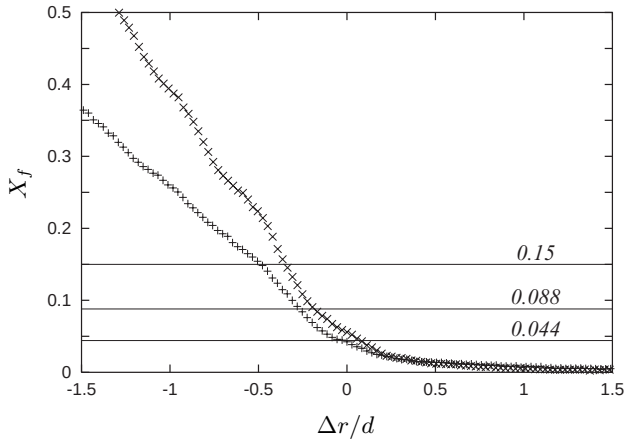

FIGURE 6. Averaged mixture fraction profiles immediately upstream of the instantaneous leading points. Δr measures the radial distance relative to the leading point. The stoichimetric value of X_f and the lean and rich flammability limits are indicated. +, case 1, ×, case 2.

points) for either side of the centerline are collected in Fig. 5. For case 1, the mean position of these points is found at $x = 11.5\,d$, $r = 2.3\,d$; for case 2, the mean position is $x = 8.6\,d, r = 1.9\,d$. As indicated in Fig. 3, these x values closely match the points at which the flow width, δ, deviates from its linear evolution.

As mentioned above, the structure of an edge flame is highly dependent on the incoming velocity and fuel concentration profiles. Figures 6 and 7 show the averaged fuel mole fraction and axial velocity profiles upstream of the instantaneous high temperature interfaces. The profiles are compiled along lines of fixed x, lying roughly 0.5 mm upstream of the leading points. In offsetting the profiles slightly from the high temperature interfaces, it is intended that the effect of varying temperatures on fluorescence signal be minimized. (At the profile locations, temperatures should be below approximately 400 K, so temperature effects will cause the measured mole fractions to deviate by no more than

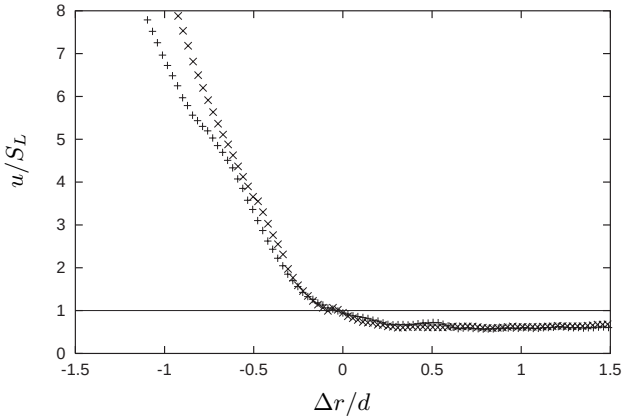

FIGURE 7. Averaged profiles of the axial velocity, normalized by the laminar flame speed, upstream of the instantaneous leading points. +, case 1, ×, case 2.

15% from the true mole fractions.) The horizontal axis of the profiles, Δr, is the radial position relative to the leading point. To interpret the fuel mole fraction profile, observe that the stoichiometric mole fraction for a methane-acetone mixture with respective mole fractions in the ratio 0.85:0.15 is 0.088. The lean flammability limit for methane (in air, at 298 K and 1 atm) lies at mole fraction 0.050, and for acetone lies at 0.026 (Glassman (1987)), so by Le Chatelier's principle, the lean flammability limit for the mixture is at mole fraction 0.044. The rich flammability limits are 0.15 mole fraction for methane and 0.13 for acetone. Immediately upstream of the leading point ($\Delta r = 0$), the fuel mole fraction is approximately the lean flammability limit for case 1, at a value of 0.042, and is slightly above the lean limit, at 0.056, for case 2. The fuel fraction quickly drops below the lean flammability limit towards the outside of the jet (positive Δr). Towards the inside of the jet, the fuel fraction gradient increases sharply. The stoichiometric point for case 1 is $\Delta r = -0.28$ and for case 2 is $\Delta r = -0.2$, and the fuel fraction exceeds 0.15 at $\Delta r = -0.42$ for case 1 and -0.36 for case 2. The profile for case 2 shows a higher gradient than that for case 1, owing to the smaller average jet width at the lower liftoff height for case 2.

The profiles of mean axial velocity, u, upstream of the instantaneous leading points for the two cases are shown in Fig. 7. Values are normalized by 0.43 m/s, the stoichiometric laminar burning velocity of both methane and acetone (Glassman (1987)). Immediately upstream of the leading point, the axial velocity is slightly below S_L. Towards the outside of the jet, the axial velocity profile drops below both S_L and the coflow velocity, indicating a deceleration of the flow upstream of the high temperature region. On the inside of the jet, the axial velocity rises steeply, with the higher gradient being seen for the case 2 profiles, as with the fuel fraction profiles shown above.

From probability distributions (not shown) of the axial velocity, u, at various positions on the high temperature interface determined from the Mie scattering images, statistics of the incoming fluid velocities can be compiled. We define the '0' position as on the interface, with Δr (relative to the leading point) between -1 and 1 mm. The '-' position is on the interface towards the jet centerline, -3 mm $< \Delta r <$ -1 mm, and the '+' position is on the interface to the outside of the jet, 1 mm $< \Delta r <$ 3 mm. (These positions are indicated in Fig. 1.) Immediately around the leading point (the '0' position) the velocities average near S_L, with averages of 0.86 S_L for case 1 and 0.95 S_L for case 2. Towards the

centerline (the '-' position) the average axial velocity increases, to 2.02 S_L for case 1 and 2.51 S_L for case 2. Away from the centerline (the '+' position), the velocities average 0.51 S_L for case 1 and 0.58 S_L for case 2, indicating that the flow in that region has decelerated from the coflow speed of 0.84 S_L.

2.3. *Discussion*

The profiles of fuel mole fraction and axial velocity immediately upstream of the high temperature regions (Figs. 6 and 7) are instructive in the context of theories of edge flames. The assumption that the leading point of these regions corresponds to a stoichiometric mixture with fuel-lean conditions to the outside and rich conditions to the inside is not supported here. Instead, the average fuel mole fraction at the leading point is near the lean flammability limit. The sample scalar field of Fig. 2 illustrates this point; the high temperature interface to the left of the centerline seems to show no fuel to the outside of the leading point, while the interface to the right of centerline shows low fuel concentrations to the outside. In general, the portion of the high temperature interface outside of the leading point will have insufficient fuel fraction to support combustion. Instead, it appears that flammable mixtures, and the flame zone position, are biased towards the inside of the high temperature regions.

This conclusion is in agreement with the simultaneous CH/OH PLIF measurements in lifted flames of Watson *et al.* (1999a), in which the CH zones were found to lie on the inner boundaries of the OH zones, and the more recent CH PLIF measurements by the same authors (Watson *et al.* (1999b)), which showed evidence of weak CH zones (thought to correspond to the lean premixed branch) curling outward from the bases of the primary CH zones (thought to correspond to the diffusion branch). These latter measurements were not performed simultaneously with OH PLIF, but it can be inferred that the weaker CH zones correspond to the region of the high temperature interface near and to the outside of the leading point. This lean premixed branch was only observed in roughly 30% of the images, which Watson *et al.* attributed to three-dimensional effects. The present measurements suggest that the absence of a lean premixed branch can be explained by the incoming fuel mixture fractions being below the flammability limit.

While the lean premixed branch of the idealized triple flame has been observed through CH imaging, the fuel-rich branch has not. Watson *et al.* (1999b) cite the simulations of Veynante *et al.* (1994), which demonstrate that incoming vortices can distort the edge flame in such a way that one or both of the premixed branches is obscured. This notion is supported by the axial velocity profiles upstream of the leading point (Fig. 7). The profiles show a strong velocity gradient consistent with a vortex which draws ambient fluid into the jet from below and moves jet fluid upward and away from the centerline. Such a vortex might possibly fold the rich premixed branch of an edge flame into the diffusion tail (Veynante *et al.* (1994)).

The axial velocity statistics discussed above indicate that velocities upstream of the high temperature interfaces are relatively low, consistent with previous observations (Muñiz & Mungal (1997), Schefer & Goix (1998), Watson *et al.* (1999a)). The actual values are, however, somewhat lower than those reported by Muñiz & Mungal or Watson et al. Schefer & Goix found that the incoming velocities diminished with lower jet Reynolds numbers. This was attributed to lower liftoff heights observed for the lower Re. At the lower positions, flammable layers are thinner, resulting in greater flame curvature and, it was concluded, less efficient preheating of reactants. The present Reynolds numbers are indeed lower than those of Muñiz & Mungal and Watson *et al.* However, the full set of current measurements encompasses a range of Reynolds numbers up to roughly 10000.

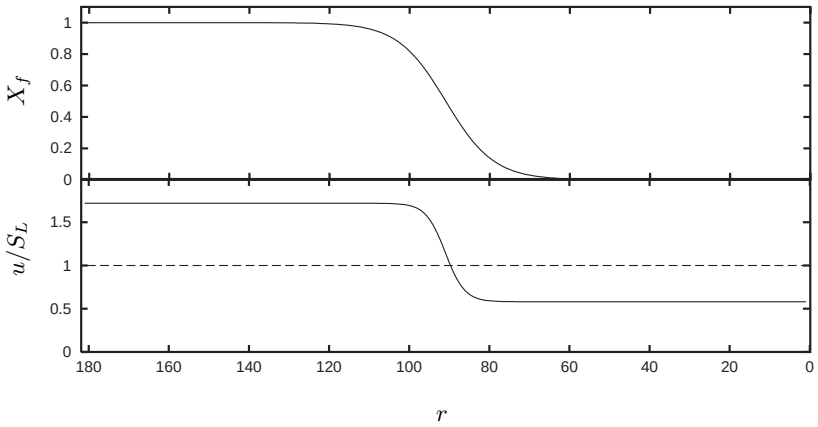

FIGURE 8. Inflow profiles of mixture fraction and axial velocity used in the edge flame simulation.

Analysis of this set in its entirety will permit an assessment of the effects of these issues of flammability layer thickness and flame curvature.

3. Future work

Preliminary work is underway to use the measured fuel mole fraction and axial velocity profiles from these experiments in the edge flame code of Ruetsch (Veynante *et al.* (1994), Ruetsch *et al.* (1995)). The resulting reaction rate fields can then be compared with those observed experimentally, for example by Watson *et al.* (1999b), using measurements of the CH radical. This comparison will shed some light on the ability of the simple edge flame formulation with laminar flow fields and simplified chemistry to describe the stabilization phenomenon in lifted, turbulent diffusion flames.

The code of Ruetsch computes the fully compressible, 2-D Navier-Stokes equations, and incorporates the single-step, irreversible reaction $F + O \rightarrow P$. The simulation is initialized with a premixed line flame of specified thickness δ_0. The non-uniform mixture fraction and velocity profiles are introduced at the inflow boundary. An initial run has been performed using the experimental results presented in this paper as inputs to the simulation. For this run, we use hyperbolic tangent profiles for the velocity and mixture fraction profiles. We define δ_u and δ_X as the inverses of the slopes of the velocity and mixture fraction profiles, respectively, at the stoichiometric point. The ratios δ_u/δ_0 and δ_X/δ_0 are determined from the experimental profiles presented in Figs. 6 and 7.

The tanh inflow profiles used in the initial run are shown in Fig. 8. Contours of the reaction rate field at two later times are shown in Fig. 9. The incoming flow moves from bottom to top in the figures. Some tentative observations can be made. First, the flame migrates away from the initial stoichiometric location in fuel-lean regions, consistent with the present experiments. Secondly, for the later of the two times shown, the highest reaction rate on the flame leading edge (which corresponds to the local stoichiometric position) does not correspond to the leading point as defined in this paper, as has also been suggested by Chen *et al.* (2000). Finally, the configuration of the premixed flame branches begins to resemble the CH fields observed by Watson *et al.* (1999b). In particular, the fuel-rich branch for the later of the two times appears to

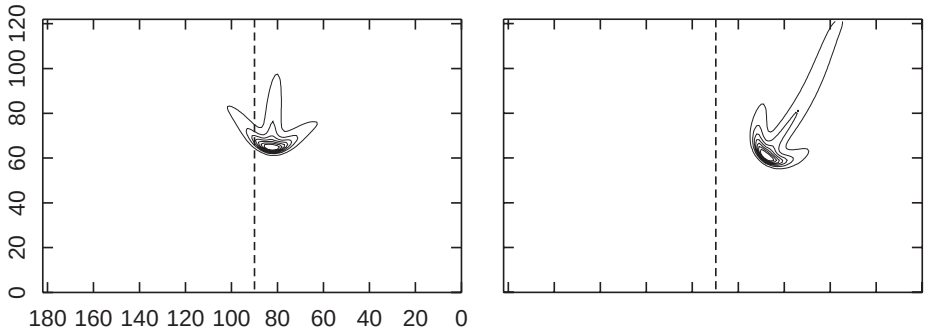

FIGURE 9. Reaction rate contours from the simulation at early (left) and later (right) times. The dashed line in each plot indicates the initial stoichiometric position. Axes represent simulation grid points.

be aligned roughly parallel to the incoming flow, while the fuel-lean branch is roughly normal to the incoming flow, curling up slightly at the extreme lean side.

These results, while far from conclusive, suggest that this laminar edge flame model with simple chemistry is well able to reproduce significant features seen in experimental lifted turbulent jet diffusion flames. Issues to be addressed in future work include carrying the simulation out to longer times, incorporating more realistic inflow profiles, and using inflow parameters from experimental results at different Reynolds numbers.

REFERENCES

BILGER, R. W. 1982 Molecular transport effects in turbulent diffusion flames at moderate Reynolds numbers. *AIAA J.* **20**, 962-970.

CHEN, M., HERRMANN, M. & PETERS, N. 2000 Flamelet modeling of lifted turbulent methane/air and propane/air turbulent jet diffusion flames. *Proc. Twenty-Eighth Symp. (Int'l) on Combustion, The Combustion Institute, Pittsburgh, PA.*

DOLD, J. W. 1989 Flame propagation in a nonuniform mixture: analysis of a slowly varying triple flame. *Comb. Flame.* **76**, 71-88.

GLASSMAN, I. 1987 *Combustion (2nd ed.),* Academic Press, Orlando, FL, 1987.

HASSELBRINK, E. F. 1999 *Transverse Jets and Jet Flames: Structure, Scaling, and Effects of Heat Release. Report No. TSD-121,* Thermosciences Division, Stanford University.

HASSELBRINK, E. F. & MUNGAL, M. G. 1998 Characteristics of the velocity field near the instantaneous base of lifted non-premixed turbulent jet flames. *Proc. Twenty-Seventh Symp. (Int'l) on Combustion, The Combustion Institute, Pittsburgh, PA* 867-873.

KELMAN, J. B., ELTOBAJI, A. J. & MASRI, A. R. 1998 Laser imaging in the stabilisation region of turbulent lifted flames. *Comb. Sci. Tech.* **135**, 117-134.

MAUREY, C., CESSOU, A. & STEPOWSKI, D. 1998 Simultaneous PIV and OH planar LIF in the stabilization region of a lifted turbulent jet flame. *Proc. 9th Int'l Symp. on Appl. of Laser Techniques to Fluid Mech., Lisbon*, 25.3.1-25.3.8.

MÜLLER, C. M., BREITBACH, H. & PETERS, N. 1994 Partially premixed turbulent flame propagation in jet flames. *Proc. Twenty-Fifth Symp. (Int'l) on Combustion, The Combustion Institute, Pittsburgh, PA* 1099-1106.

Muñiz, L. & Mungal, M. G. 1997 Instantaneous flame-stabilization velocities in lifted-jet diffusion flames. *Comb. Flame* **111**, 16-31.

Peters, N. & Williams, F. A. 1983 Liftoff characteristics of turbulent jet diffusion flames. *AIAA J.* **21**, 423-429.

Pitts, W. M. 1988 Assessment of theories for the behavior and blowout of lifted, turbulent-jet flames. *Proc. Twenty-Second Symp. (Int'l) on Combustion, The Combustion Institute, Pittsburgh, PA*. 809-816.

Reid, R. C., Prausnitz, J. M. & Poling, B. E. 1987 *The Properties of Gases and Liquids (4th ed.).* McGraw- Hill, New York.

Ruetsch, G. R., Vervisch, L. & Liñán, A. 1995 Effects of heat release on triple flames. *Phys. Fluids.* **7**, 1447-1454.

Schefer, R. W., Namazian, M. & Kelly, J. 1994 Stabilization of lifted turbulent-jet flames. *Comb. Flame.* **99**, 75-86.

Schefer, R. W. & Goix, P. J. 1998 Mechanism of flame stabilization in lifted, turbulent-jet flames. *Comb. Flame.* **112**, 559-574.

Su, L. K., Han, D. & Mungal, M. G. 2000 Measurements of velocity and fuel concentration in the stabilization region of lifted jet diffusion flames. *Proc. Twenty-Eighth Symp. (Int'l) on Combustion, The Combustion Institute, Pittsburgh, PA.*

Thurber, M. C. 1999 *Acetone Laser-Induced Fluorescence for Temperature and Multiparameter Imaging in Gaseous Flows. Report No. TSD-120,* Thermosciences Division, Stanford University, 1999.

Vanquickenborne, L. & van Tiggelen, A. 1966 The stabilization mechanism of lifted turbulent diffusion flames. *Comb. Flame.* **10**, 59-69.

Veynante, D., Vervisch, L., Poinsot, T., Liñán, A. & Ruetsch, G. R. 1994 Triple flame structure and diffusion flame stabilization. *Summer Program Proceedings*, Center for Turbulence Research, NASA Ames/Stanford Univ. 55-73.

Watson, K. A., Lyons, K. M., Donbar, J. M. & Carter, C. D. 1999a Scalar and velocity field measurements in a lifted CH_4-air diffusion flame. *Comb. Flame.* **117**, 257-271.

Watson, K. A., Lyons, K. M., Donbar, J. M. & Carter, C. D. 1999b Observations on the leading edge in lifted flame stabilization. *Comb. Flame.* **119**, 199-202.

Westerweel, J., Dabiri, D. & Gharib, M. 1997 The effect of a discrete window offset on the accuracy of cross-correlation analysis of PIV recordings. *Exp. Fluids.* **23**, 20-28.